UDC 004.896:629.36:658.78 DOI https://doi.org/10.35546/kntu2078-4481.2026.2.36

I. SH. NEVLIUDOV
Doctor of Technical Sciences, Professor,
Head of the Department of Computer-Integrated Technologies,
Automation, Robotics and Safety Engineering
Kharkiv National University of Radio Electronics
ORCID: 0000-0002-9837-2309

V. V. YEVSIEIEV
Doctor of Technical Sciences, Professor,
Professor at the Department of Computer-Integrated Technologies,
Automation, Robotics and Safety Engineering
Kharkiv National University of Radio Electronics
ORCID: 0000-0002-2590-7085

E. A. JABRAYILZADE
Postgraduate Student at the Department of Department of Computer-Integrated
Technologies, Automation, Robotics and Safety Engineering
Kharkiv National University of Radio Electronics
ORCID: 0000-0003-2932-4976

INTELLIGENT MOTION PLANNING OF A COLLABORATIVE MOBILE ROBOT IN A DYNAMIC ENVIRONMENT BASED ON VFH+ AND SEMANTIC PROCESSING OF LIDAR AND VIDEO DATA

The article presents results of the study aimed at developing and substantiating a method for intelligent motion planning of a collaborative mobile robot in a dynamic environment based on the VFH+ algorithm with semantic weighting of LiDAR and video camera data. The purpose of the study is to enhance the safety, predictability, and adaptability of a mobile robotic platform operating in the presence of static and dynamic obstacles through the integration of geometric environmental information with contextual risk assessment. The object of the study is the process of planning and executing the trajectory of a collaborative mobile robot within a structured workspace that includes dynamic elements typical of Human–Robot Collaboration (HRC) scenarios. The subject of the study comprises mathematical models and algorithmic procedures for generating control actions based on a polar obstacle histogram augmented with a semantic evaluation of the hazards associated with objects detected through computer vision.

The study uses a kinematic model of a differential-drive system, a method for constructing a polar obstacle grid using LiDAR data, generation and smoothing of the VFH+ histogram, sector binarization and identification of admissible motion directions, as well as a multi-criteria selection of the optimal sector considering goal orientation, smoothness, and risk level. To consider the context of interaction with humans and other objects, a semantic multiplier is introduced, which modifies the initial histogram according to the results of video detection. The numerical modeling is implemented in Python with discrete integration of motion equations, taking into account sensor noise and combining local VFH+ with global route landmarks obtained with the use of A algorithm.*

The scientific novelty is the formulation of an integrated motion planning model that combines geometric obstacle density in polar space with semantic risk weighting, that enables adaptive modification of forbidden and free sectors depending on the type and behavior of environmental objects. A mechanism for adapting binarization thresholds and weight coefficients of the direction selection criterion upon detection of jamming signs is proposed, thereby increasing the stability of the algorithm in narrow passages. The modeling results confirm that the target point is reached without loss of stability and in compliance with safe speed limits and minimum distance to obstacles, which indicates the effectiveness of combining VFH+ with semantic processing of LiDAR and video data for HRC environments.

Key words: *collaborative mobile robot, motion planning, VFH+, semantic navigation, sensor fusion, LiDAR, computer vision, obstacle avoidance, dynamic environment.*

І. Ш. НЕВЛЮДОВ
доктор технічних наук, професор,
завідувач кафедри комп'ютерно-інтегрованих технологій,
автоматизації, робототехніки та безпекової інженерії
Харківський національний університет радіоелектроніки
ORCID: 0000-0002-9837-2309

© I. Sh. Nevliudov, V. V. Yevsieiev, E. A. Jabrayilzade, 2026
Стаття поширюється на умовах ліцензії відкритого доступу CC BY 4.0 ISSN 2078-4481

В. В. ЄВСЄЄВ
доктор технічних наук, професор,
професор кафедри комп'ютерно-інтегрованих технологій,
автоматизації, робототехніки та безпекової інженерії
Харківський національний університет радіоелектроніки
ORCID: 0000-0002-2590-7085

Е. А. ДЖАБРАЙІЛЗАДЕ
аспірант кафедри комп'ютерно-інтегрованих технологій,
автоматизації, робототехніки та безпекової інженерії
Харківський національний університет радіоелектроніки
ORCID: 0000-0003-2932-4976

ІНТЕЛЕКТУАЛЬНЕ ПЛАНУВАННЯ РУХУ КОЛАБОРАТИВНОГО МОБІЛЬНОГО РОБОТА В ДИНАМІЧНОМУ СЕРЕДОВИЩІ НА ОСНОВІ VFH+ ТА СЕМАНТИЧНОЇ ОБРОБКИ LIDAR ТА ВІДЕОДАНИХ

У статті представлено результати дослідження, спрямованого на розроблення та обґрунтування методу інтелектуального планування руху колаборативного мобільного робота в динамічному середовищі на основі алгоритму VFH+ із семантичним зважуванням даних LiDAR та відеокамери. Метою роботи є підвищення безпечності, передбачуваності та адаптивності руху мобільної роботизованої платформи за наявності статичних і динамічних перешкод шляхом інтеграції геометричної інформації про оточення з контекстною оцінкою ризику. Об'єктом дослідження є процес планування та реалізації траєкторії переміщення колаборативного мобільного робота в структурованому робочому просторі з елементами динаміки, характерними для HRC-сценаріїв. Предмет дослідження становлять математичні моделі та алгоритмічні процедури формування керуючих впливів на основі полярної гістограми перешкод, доповненої семантичною оцінкою небезпеки об'єктів, що виявляються засобами комп'ютерного зору.

У роботі застосовано кінематичну модель диференціального приводу, метод побудови полярної сітки перешкод за даними LiDAR, формування та згладжування гістограми VFH+, бінаризацію секторів і виділення допустимих напрямків руху, а також багатокритеріальний вибір оптимального сектора з урахуванням цілеспрямованості, плавності та рівня ризику. Для врахування контексту взаємодії з людиною та іншими об'єктами введено семантичний множник, який модифікує первинну гістограму відповідно до результатів відеодетекції. Чисельне моделювання реалізовано в середовищі Python із дискретною інтеграцією рівнянь руху, урахуванням сенсорного шуму та поєднанням локального VFH+ з глобальними орієнтирами маршруту, отриманими за алгоритмом A.*

Наукова новизна полягає у формуванні інтегрованої моделі, що поєднує геометричну щільність перешкод у полярному просторі із семантичним зважуванням ризику, забезпечуючи адаптивну зміну структури заборонених і вільних секторів залежно від типу та поведінки об'єктів. Запропоновано механізм адаптації порогів бінаризації та вагових коефіцієнтів критерію вибору напрямку при виявленні ознак застрягання, що підвищує стійкість алгоритму у вузьких проходах. Результати modeling підтверджують досягнення цільової точки без втрати стабільності та з дотриманням безпечних обмежень швидкості й мінімальної дистанції до перешкод, що свідчить про ефективність поєднання VFH+ із семантичною обробкою LiDAR та відеоданих для HRC-середовищ.

Ключові слова: *колаборативний мобільний робот, планування руху, VFH+, семантична навігація, сенсорна фузія, LiDAR, комп'ютерний зір, уникнення перешкод, динамічне середовище.*

Introduction

The fast development of Industry 5.0 is leading to the active use of collaborative mobile robots in manufacturing, logistics, and service processes, where they work directly with people [1-3]. In such conditions, the problem of safe and adaptive motion planning in a dynamic environment with uncertain obstacles and variable space configuration becomes particularly relevant [4-7]. Traditional navigation methods based solely on geometric information do not always provide a sufficient level of predictability and semantic understanding of the scene, which is critically important in Human–Robot Collaboration (HRC) scenarios [8-10]. The integration of Light Detection and Ranging (LiDAR) data with video information opens up opportunities for forming a more informative model of the environment, taking into account the type of objects and the level of potential risk [11-12]. The Vector Field Histogram Plus (VFH+) method, as an effective approach to local planning, enables fast real-time decision-making, and its extension with semantic weights improves the quality of selecting safe movement directions [13-15]. Thus, the development of an intelligent motion planning method based on a combination of a polar histogram of obstacles and semantic processing of sensor data is necessary to improve the reliability, safety, and adaptability of collaborative mobile robots in complex dynamic environments.

Analysis of recent studies and publications

The intensive development of collaborative robotics and Industry 5.0 concepts is driving a growing need for intelligent methods of planning the movement of mobile robots capable of operating in dynamic environments involving humans.

Current research focuses on combining classical geometric obstacle avoidance algorithms with semantic scene interpretation, which opens up opportunities for improving navigation safety and adaptability. In this regard, it is relevant to analyze existing approaches to the use of VFH+, Light Detection and Ranging (LiDAR), and video data to justify the need for an integrated model of semantically weighted motion planning for collaborative mobile robots.

In their work, Liang, Ji, and others proposed a multi-agent VFH+ type control for "flocking" with a mechanism for exiting dynamic equilibrium (when a group can "hang" near complex obstacles), which makes it possible to reduce the risk of collective local minima and stabilize the movement of a group of robots in dense obstacle configurations [16]. However, this approach is difficult to use directly, as it is focused on agent-agent interaction and formation support, rather than on contextual (semantic) risk assessment of objects and stable passage of narrow wall "heads" with Line-Of-Sight Override (LOS-override), which was a critical cause of jamming in our modeling.

In their work, Rose, McMurray, and others developed FALCON, a field-oriented approach to autonomous LiDAR-based obstacle avoidance that allows control actions to be formed through a "field" of navigational influences and supports avoidance in complex geometry [17]. However, the proposed solution does not take into account semantic weighting (the type of risk of an object from video detection) and in HRC scenarios can produce undesirable behavior when a "geometrically permissible" direction is contextually dangerous (a person or dynamic agent in the area).

In the article by Hu and Gan, semantic navigation for robotic inspection and environmental quality monitoring in indoor spaces is investigated, where semantics is used to interpret the scene and select the robot's behavior, which increases the meaningfulness of navigation decisions compared to purely geometric methods [18]. It should be noted that inspection scenarios often allow for slower planning contours and other optimality criteria, which means that the mechanisms described in the article do not automatically provide stability against looping at the ends of walls.

Gutiérrez-Álvarez, Ríos-Navarro, et al. demonstrate an approach to visual semantic navigation on real robots using semantic scene features to achieve goals in rooms, which makes it possible to move from an "obstacle map" to a "meaning map" and increase robustness in complex environments [19]. However, visual semantic schemes without a polar histogram often require different infrastructure (semantic maps, training, other control contours) and do not guarantee minimum distance control and smooth commands in narrow "corridors" without additional stabilizers.

In their publication, Shen, Luo, and others propose enhancing multi-agent semantic navigation through multimodal collaboration and scoring with chain-of-thought elements to coordinate decisions between agents, which can improve the quality of action selection through collective information sharing [20]. However, this is difficult to apply in real time on a single robot with a limited computing budget and a direct conversion of "LiDAR+video → polar histogram → command," while multimodal Chain-of-Thought collaboration (CoT-collaboration) usually requires more delay, more complex communication, and a different level of architecture that does not meet the requirement for fast local obstacle avoidance in HRC.

The article by Yang, An, et al. provides an overview of collision avoidance coordination in multi-robot systems, systematizes approaches, and highlights typical problems of local minima and trade-offs between safety and performance [21]. However, the review nature of the work does not provide a ready-made mechanism for integrating semantic risk specifically into VFH+ with adaptation of the binarization threshold and LOS override, which was crucial for eliminating "circular twisting" in the "head" area of the model walls.

In their study, Wei, Wang, and others analyzed Robot Operating System (ROS)-oriented navigation and obstacle avoidance architectures, methods, and trends, which helps to justify the choice of modules and typical pipelines in robotic systems [22]. However, this is more of a basis for positioning a solution than a direct methodological replacement, because ROS architectures describe "how to integrate" rather than "how to calculate polar sectors with risk and ensure escape from traps."

In their work, Misir and Celik propose a visual obstacle avoidance method based on extended CNNs, which makes it possible to train the model to recognize dangerous situations and generate reactive control decisions based on images [23]. However, the proposed Convolutional Neural Network (CNN)-only scheme without LiDAR may lose the metric "guarantee" of distance to obstacles and require significant datasets/retraining for new scenes, which is undesirable for HRCs with rapid changes in the environment.

In their article, Sousa, Silva, and others investigated obstacle avoidance techniques for mobile robots in autonomous warehouse HRC environments, where dense traffic, human presence, and production safety constraints are important [24]. However, direct transfer of the approach to this study may be limited due to differences in the scenario (warehouse logistics, specific interaction rules, and movement maps) and because this study focuses on a universal local reactive VFH+ scheme with semantic sector modification and local minimum elimination mechanisms (adaptive thresholds, reverse-escape, LOS-override) that specifically "treat" traps near walls.

In general, the analysis shows that modern robots either delve into multi-robot coordination, or into semantic navigation with a predominance of visual/training components, or into architectural surveys, but do not completely solve the practical problem typical for HRC: stable real-time avoidance of obstacles in narrow passages while taking into account semantic risk, which confirms the necessity and relevance of your research as a "bridge" between geometrically

guaranteed VFH+ and contextually grounded (semantic) solutions that reduce the risk of dangerous encounters in a dynamic environment.

Statement of the task

The aim of the study is to improve the safety, predictability, and adaptability of a mobile robotic platform's movement in the presence of static and dynamic obstacles by integrating geometric information about the environment with contextual (semantic) risk assessment.

Presentation of the main material

The Vector Field Histogram Plus (VFH+) method is an advanced local motion planning algorithm that generates a polar histogram of obstacle density based on sensor data and determines a safe motion direction, taking into account the robot's kinematic constraints and the width of passable "valleys" [25]. Its distinctive feature is the combination of high speed, real-time operation, and the ability to take into account the dimensions and dynamics of the platform, which is critical for collaborative mobile robots in environments with people. In the context of intelligent motion planning, the integration of VFH+ with semantic processing of LiDAR and video data allows not only to assess geometric hazards, but also to take into account the type of object and the level of interaction risk. This increases the adaptability and predictability of the robot's behavior in a dynamic environment and justifies the need for further research in the direction of sensor fusion and semantically oriented trajectory planning.

Let's describe the robot's state model as a vector $\boldsymbol{x}_k$ in discrete time. This is necessary in order to move from the selected direction (from VFH+) to the actual control of the robot and predict its position one step ahead:

$$\boldsymbol{x}_k = \begin{bmatrix} x_k \\ y_k \\ \theta_k \end{bmatrix}, \ \Delta t > 0 \tag{1}$$

Where: $\boldsymbol{x}_k$ – vector describing the spatial position and orientation of a mobile platform at a discrete point in time k; x_k, y_k – determines the coordinates of the robot's center in the selected reference frame, which are used to construct the trajectory and estimate the distance to the target and obstacles; θ_k – characterizes the angle of orientation relative to the coordinate axis, which affects the direction of further movement; $\Delta t > 0$ – discretization step, that sets the time interval for model updates, determines the frequency of real-time control action recalculation and ensures numerical implementation of the motion planning algorithm (VFH+ update frequency, e.g., 10–20 Hz).

The kinematic model of the differential drive, necessary to convert the direction of motion selected by the VFH+ method into specific control actions of linear and angular velocity, taking into account the real kinematic limitations of the mobile platform. It provides accurate prediction of changes in the robot's position and orientation over time, allowing for the assessment of movement stability and safety in a dynamic environment. This achieves consistency between the intelligent choice of direction and the physically realized trajectory of movement:

$$\begin{aligned} x_{k+1} &= x_k + v_k cos\theta_k \Delta t \\ y_{k+1} &= y_k + v_k sin\theta_k \Delta t \\ \theta_{k+1} &= \theta_k + w_k \Delta t \end{aligned} \tag{2}$$

Where: x_{k+1} – predicted value of the coordinate along the axis X after performing control actions during Δt; y_{k+1} – predicted value of the coordinate along the axis Y after performing control actions during Δt; θ_{k+1} – predicted value of robot orientation after angular velocity action during the interval Δt; v_k – linear speed of the platform at a given moment in time k, that forms the displacement value for the interval Δt; w_k – angular rotation speed of the robot, which determines the change in its orientation per time step.

A LiDAR sensor model with a transition to a polar grid of obstacles is necessary for a structured representation of spatial information about the environment in the form of angular sectors relative to the robot [26]. It allows converting the array of measured distances into a compact form of a polar histogram, which is the basis for the VFH+ algorithm. Thanks to this model, it is possible to quickly determine directions with increased obstacle density and form safe movement sectors in real time.

Let LiDAR provide measurements $\{(r_i, \phi_i)\}_{i=1}^{N}$ in the coordinate system of the collaborative robot, where: r_i – range and ϕ_i – beam angle. We divide the field of view into M sectors with a width of α:

$$\alpha = \frac{\Phi_{max} - \Phi_{min}}{M} \tag{3}$$

$$j(\phi_i) = \frac{\phi_i - \Phi_{min}}{\alpha}, \ j \in \{0, \ldots, M-1\}$$

Where: α is the angular width of one sector of the histogram, which determines the resolution of the space

representation; Φ_{max} – maximum LiDAR viewing angle, which sets the final boundary of the scanning area; Φ_{min} – minimum LiDAR viewing angle in the selected coordinate system, which determines the initial boundary of the analyzed space sector; M – number of sectors of the polar histogram into which the angular range is discretized to form the interference grid; ϕ_i – angle of a separate LiDAR laser beam relative to the robot axis for which the range measurement was obtained; $j(\phi_i)$ – index of the polar histogram sector to which the measurement with angle ϕ_i belongs, which provides grouping of data by directions; $j \in \{0,\ldots,M-1\}$ – the permissible range of sector indices corresponding to the full angular coverage of the sensor.

Then the distance to the nearest obstacle in the sector:

$$d_j = \min_{i:\, j(\phi_i)=j} r_i \tag{4}$$

Where: d_j – minimum distance to an obstacle in a sector j, which is defined as the smallest value among all r_i belonging to this sector and is used to assess the level of danger of the direction of movement; r_i – LiDAR measured distance to the object for a beam with an index i, characterizing the actual distance to the obstacle in the corresponding direction; j – the index of the histogram sector corresponding to a specific angular interval of the analyzed space.

To take into account the actual dimensions of the mobile platform and the necessary safety margin when forming safe movement directions, the following model of obstacle inflation under the robot's dimensions is proposed. Since VFH works in directions to take into account the robot's dimensions and safety margin, we introduce a critical distance:

$$d_{safe} = R_{robot} + R_{margin} \tag{5}$$

Where: d_{safe} – critical safe distance to an obstacle, which is defined as the sum of the robot's radius and safety margin and is used to classify sectors as potentially dangerous during motion planning; R_{robot} – the effective radius of a mobile robot, which takes into account its geometric dimensions and determines the minimum space required for physical passage without collision; R_{margin} – additional safety radius, which defines a protective zone around the robot, taking into account sensor errors, control delays, and requirements for safe interaction with humans. Then we consider the sector potentially dangerous if $d_j \le d_{safe}$.

To quantitatively assess the density of obstacles in each angular sector around the robot, the following model for constructing a primary polar histogram in the VFH+ method is proposed. It converts the measured LiDAR distances into weight values that reflect the degree of danger of movement in a particular direction. This results in a compact and computationally efficient representation of space that is suitable for real-time operation.

$$H_j = \begin{cases} w_d\left(\dfrac{1}{d_j} - \dfrac{1}{d_{max}}\right), & d_j \le d_{max} \\ 0, & d_j > d_{max} \end{cases} \tag{6}$$

Where: H_j – the value of the polar histogram in the sector j, which reflects the degree of danger of movement in a given direction and is used for further selection of a safe course; w_d – weight coefficient of the distance to the obstacle, which determines the sensitivity of the algorithm to nearby objects; d_j – minimum distance to an obstacle in the sector j, minimum distance to an obstacle in the sector, received from LiDAR data, characterizing the actual level of threat in this direction; d_{max} – boundary distance for considering obstacles, beyond which the influence of objects on the histogram is considered insignificant or zero; $\left(\dfrac{1}{d_j} - \dfrac{1}{d_{max}}\right)$ – increasing weight function for closer obstacles, which provides a greater contribution of dangerous objects to the formation of the histogram.

In numerical modeling, it is convenient to take d_{max} as the LiDAR working range (for example, 6–10 m) so that the histogram does not "stick" to distant walls.

Complementing LiDAR geometric information with contextual understanding of the type of objects in the robot's field of view, we propose using a camera-based semantic risk weighting model. Within the scope of this study, it allows us to differentiate obstacles by their level of potential danger, giving greater weight to directions where people or critical objects are detected. In other words, LiDAR sees geometry well, while the camera sees the class of the object (person, vehicle, risk zone). In VFH+, this can be entered as an additional weighting factor. Let's get a set of objects $\mathcal{O}$ from the camera, and for each we have: angular interval $\left[\phi_0^-, \phi_0^+, \right]$ and assessment of risk or significance $s_o \in [0,1]$, as an example, "human" is closer to 1. Then the semantic multiplier for the sector will look like this:

$$S_j = 1 + w_s \sum_{o \in \mathcal{O}} s_o \cdot 1\left\{\phi_j \in \left[\phi_0^-, \phi_0^+, \right]\right\} \tag{7}$$

Where: S_j – semantic weight coefficient for the sector j, which modifies the polar histogram values taking into

account the type of objects in the corresponding direction; w_s – the coefficient of semantic information influence, which determines how strongly the results of video analysis change the navigation decision; $\mathcal{O}$ – a set of objects detected by the camera in the current frame that are taken into account when assessing risk; s_o – semantic assessment of risk or priority for an object o, reflecting the degree of its potential danger to the movement of the robot; ϕ_j – the central angle of the sector j in the polar histogram, which determines the corresponding direction of movement; $\left[\phi_0^-, \phi_0^+, \right]$ – angular interval within which the object o is located relative to the robot; $1\left\{\phi_j \in \left[\phi_0^-, \phi_0^+, \right]\right\}$ – indicator function, which takes the value 1 if the sector direction falls within the object's location area, and 0 otherwise, ensuring selective consideration of semantic influence.

Final histogram taking into account the camera:

$$\tilde{H}_j = H_j \cdot S_j \tag{8}$$

Where: $\tilde{H}_j$ – the final value of the polar histogram in the sector j, that takes into account both the geometric density of obstacles and the semantic risk assessment, and is used to select a safe direction of movement; H_j – the base value of the histogram, formed on the basis of LiDAR data, reflecting the degree of proximity of obstacles in the sector j; S_j – semantic correction coefficient for the sector j, that modifies the geometric assessment taking into account the type of detected objects and their potential level of danger; j – index of the angular sector of the polar grid corresponding to a specific direction relative to the robot.

The histogram smoothing model in VFH+ is used to reduce the impact of LiDAR noise and the instability of semantic estimates from the camera on the process of selecting the direction of movement. In this study, it stabilizes control decisions, preventing sharp trajectory fluctuations with minor changes in sensor data. This improves the smoothness of movement, predictability of robot behavior, and safety of its operation in a dynamic collaborative environment. We perform smoothing with a sliding window:

$$\tilde{H}_j = \sum_{m=-L}^{L} k_m \tilde{H}_{j+m} \tag{9}$$

Where: $\tilde{H}_{j+m}$ – the value of the final histogram in neighboring sectors relative to j, which are taken into account during smoothing; m – the shift index from the central sector j, which determines the position of the neighboring element within the smoothing window; L – the smoothing window radius, which specifies the number of sectors on each side that participate in filtering and determines the degree of averaging; k_m – smoothing kernel weight coefficients, which determine the contribution of each neighboring sector to the formation of the smoothed value and are usually normalized so that their sum is equal to one; j – the index of the current sector of the polar histogram for which the smoothed value is calculated.

To convert the quantitative assessment of obstacle density into a qualitative classification of directions as “free” or “prohibited,” a histogram binarization model is proposed. Within the framework of this study, it allows us to identify safe angular sectors suitable for further analysis and selection of the optimal direction of movement. This creates a basis for searching for passable “valleys” in accordance with VFH+ requirements and safe navigation conditions. Threshold:

$$B_j = \begin{cases} 1, \hat{H}_j \geq T \\ 0, \hat{H}_j < T \end{cases} \tag{10}$$

Where: B_j – binary value for the sector j, which determines its status as prohibited (1) or free (0) direction of movement; $\hat{H}_j$ – smoothed value of the polar histogram in the sector j, reflecting the integral estimate of interference density, taking into account semantic correction and noise filtering; T – the danger threshold value used to classify sectors and determine the acceptable risk level during motion planning.

The VFH+ valley detection model is used to determine continuous angular intervals in which robot motion is potentially safe after histogram binarization [16]. Within the scope of this study, “valleys” are continuous angular intervals of the polar histogram in which the obstacle density value does not exceed the set danger threshold and which are classified as free for movement. They are formed after binarization of the smoothed histogram and reflect potentially passable directions relative to the current position of the robot. The model allows us to evaluate not only the presence of a free direction, but also the sufficiency of its width, taking into account the dimensions of the platform and the safety margin. Analysis of the angular width of the passage prevents the selection of overly narrow sectors that can lead to collisions or unstable maneuvering. Let the “valley” be a sequence of sectors $\left[j_a, j_b\right]$ де $B_j = 0$.

Angular width of the valley:

$$\Delta\phi = \left(j_b - j_a + 1\right)\alpha \tag{11}$$

Where: $\Delta\phi$ – angular width of the “valley,” which characterizes the size of the continuous free interval of directions

suitable for safe movement of the robot; j_a – index of the initial "valley" sector, which defines the left boundary of the free angular interval; j_b – index of the final sector of the "valley," which sets the right boundary of the passable direction; α – angular width of one sector of the polar histogram, which determines the resolution of space discretization; $(j_b - j_a + 1)\alpha$ – the number of sectors that make up the "valley", and their product of α gives the actual angular value of the available passage.

The minimum angular width to pass at a distance d :

$$\Delta\phi_{min}(d) \approx 2arctan\left(\frac{R_{robot} - R_{margin}}{d}\right) \tag{12}$$

Where: $\Delta\phi_{min}(d)$ – minimum permissible angular width of the path at a distance d , which determines whether there is enough space for the robot to pass safely; R_{robot} – effective radius of a mobile platform, taking into account its overall dimensions when assessing passability; R_{margin} – additional safety margin that compensates for sensor errors, control delays, and requirements for safe interaction with humans; d – distance to the nearest obstacles within the valley where the geometric possibility of passing is assessed; $2\arctan(\cdot)$ – function for geometric estimation of the angular clearance required to pass between obstacles at a distance d , taking into account the ratio of the robot's dimensions to the width of the passage.

The "valley" is acceptable if:

$$\Delta\phi \geq \Delta\phi_{min}(d^*) \tag{12}$$

Where: $\Delta\phi$ – angular size of the "window" of motion; d^* – characteristic distance in the "valley" at which we estimate the width (selected in modeling).

To make a final navigation decision among all permissible "valleys" in the polar histogram, it is necessary to develop a model for determining the goal direction and a function for selecting the optimal sector. It provides a compromise between goal orientation, traffic safety, and trajectory smoothness, taking into account the previous state of the system. This allows to form an intelligently justified direction of movement, adapted to the conditions of a dynamic collaborative environment, i.e., among all permissible directions, choose the one that best leads to the goal and does not cause sharp turns.

Direction to the goal:

$$\phi_{goal} = atan2(y_g - y_k, x_g - x_k) - \theta_k \tag{13}$$

Where: ϕ_{goal} – relative angle of direction to the goal in the robot's coordinate system, which determines the desired movement orientation, taking into account the current orientation of the platform; x_g, y_g – coordinates of the goal point in the global reference system, which define the final or intermediate position of the route; x_k, y_k – current coordinates of the robot at a given moment in time k , which determine its current position in space; θ_k – current orientation angle of the robot used to transition from the global direction to the local coordinate system of the platform; $atan2(\cdot)$ – The function calculates the absolute angle to the goal in the global coordinate system, taking into account the correct quadrant definition.

Cost function: we use the classic solution for VFH+:

$$J(\phi_j) = \mu_1|\phi_j - \phi_{goal}| + \mu_2|\phi_j - \phi_{k-1}| + \mu_3\hat{H}_j \tag{14}$$

and choose:

$$\phi^* = arg\min_{\phi_j \in free} J(\phi_j) \tag{15}$$

Where: $J(\phi_j)$ – cost function for the sector j , which is used to select the optimal direction of movement by minimizing the total criterion of safety and expediency; ϕ_j – the angle corresponding to the center of the sector j in the polar histogram and is considered as a candidate direction of movement; ϕ_{goal} – desired direction to the goal, which sets the benchmark for reaching the final destination of the route; ϕ_{k-1} – the direction of movement selected in the previous step, which is taken into account to ensure smoothness and stability of the trajectory; $\hat{H}_j$ – smoothed value of the histogram in the sector j , which characterizes the density of obstacles and the level of danger in this direction; μ_1 – weight coefficient of orientation towards the goal, which determines the priority of approaching the specified point; μ_2 – smoothness coefficient, which reduces sudden changes in course and increases stability of movement; μ_3 – safety factor determining the degree of influence of obstacle density on direction selection; ϕ^* – the optimal direction of movement, selected from among the permissible sectors as one that minimizes the cost function and provides the most rational combination of safety, purposefulness, and smoothness; $free$ – a set of sectors classified as free after histogram binarization and passage width verification.

A model for converting the desired direction ϕ^* into control influences v and w necessary for implementing the

navigation solution selected by the VFH+ algorithm at the physical level of robot movement, i.e., converting ϕ^* into real drive commands. The model ensures coordination between the intelligent selection of the optimal sector and the kinematic capabilities of the mobile platform. Thanks to this, the direction of movement is transformed into permissible linear and angular velocities, taking into account dynamic constraints and safety requirements. This ensures stable, smooth, and predictable robot behavior in a real dynamic environment.

Direction error:

$$e_\phi = wrap\left(\phi^*\right) \tag{16}$$

control law:

$$\begin{gathered} w_k = sat\left(\kappa_w e_\phi, -w_{max}, w_{max}\right) \\ v_k = v_{max} \cdot \exp\left(-\kappa_v \left|e_\phi\right|\right) \cdot \sigma\left(d_{min}\right) \\ \sigma\left(d_{min}\right) = sat\left(\frac{d_{min} - d_{safe}}{d_{slow} - d_{safe}}, 0, 1\right) \end{gathered} \tag{17}$$

Where: w_k – angular velocity of the robot at a given moment in time k, which determines the intensity of rotation in the desired direction; κ_w – angular error gain, which determines the sensitivity of the control system to direction deviation; e_ϕ – angular error between the desired direction ϕ^* and current orientation of the robot; w_{max} – maximum permissible angular velocity, limiting the sharpness of the turn in accordance with the physical capabilities of the platform; $sat(\cdot)$ – saturation function, which limits the signal value within specified limits to ensure stability and traffic safety; v_k – linear speed of the robot at a step k, which determines the forward translational movement; v_{max} – maximum permissible linear speed of the mobile platform; κ_v – speed reduction coefficient depending on the angular error value, which provides deceleration during large turns; $\exp\left(-\kappa_v \left|e_\phi\right|\right)$ – exponential factor that smoothly reduces speed as deviation from the desired direction increases; d_{min} – the minimum distance to an obstacle among all sectors, which characterizes the current level of danger around the robot; $\sigma\left(d_{min}\right)$ – braking coefficient, which regulates speed depending on the proximity of obstacles; d_{safe} – critical safe distance at which speed must be reduced to a minimum; d_{slow} – the distance from which a gradual reduction in speed begins before approaching a dangerous zone; $\frac{d_{min} - d_{safe}}{d_{slow} - d_{safe}}$ – normalized obstacle proximity indicator, which determines the degree of deceleration.

The developed models provide an integrated combination of geometric and semantic information, which increases the validity of navigation decisions in a dynamic environment. They enable real-time motion planning, taking into account the kinematic constraints of the platform, the dimensions of the robot, and the requirements for safe interaction with humans. Thanks to their modular structure and mathematical formalization, the models are suitable for numerical modeling in Python and further scaling to more complex collaborative robotics scenarios.

Experimental research and analysis of the results obtained from numerical modeling

Description of hardware used for the study: CPU: 10-core Intel Core i7-1255U (1.7–4.7 GHz), GPU: Iris Xe Graphics, RAM: 16 GB, SSD: 512 GB.

Software: Windows 11 Pro (version 24H2) OS type 64-bit operating system, x64 architecture-based processor.

Development environment for numerical modeling PyCharm 2025.1.1.1 and programming language Python 3.13.7. [27-29]

The aim of the experiment is to test the performance and stability of intelligent motion planning for a collaborative mobile robot in a dynamic environment based on VFH+ with semantic weighting of LiDAR and video data to ensure safe and continuous approach to the target.

Within the experiment, the task of constructing a trajectory from the start to the "goal" point in the presence of static obstacles, vertical walls, and a moving object is solved, with the formation of local control $v(t), w(t)$ based on the results of a histogram evaluation of free directions. Additionally, the algorithm's ability to avoid "traps" and getting stuck in the end zone of walls is evaluated using global waypoint mechanisms, checking direct visibility to the target, and loop exit modes ($d_{min}(t), \sigma\left(d_{min}\right), v(t), w(t)$ and $\tilde{H}_j$.

The input data for modeling is specified as follows: the stage dimensions are $word_w$=12.0m and $word_h$=8.0m, initial robot state pose=[1.0, 1.0, 0.0] (x, y, θ), goal point goal=[11.0, 7.2], robot is modeled as a circle with radius R_{robot} =0.25m and safety margin R_{margin} =0.12m, whence d_{safe} =0.37м and d_{slow} =1.37m, integration time step dt =0.1s, maximum number of steps max_{steps} =3000, goal attainment tolerance $goal_{tol}$ =0.35m and waypoint tolerance wp_{tol} =0.55m when using lookahead=0.90м. The geometry of the environment contains boundary walls RectWall(-0.2,-0.2,12.2,0.0), RectWall(-0.2,8.0,12.2,8.2), RectWall(-0.2,0.0,0.0,8.0), RectWall(12.0,0.0,12.2,8.0) and two internal vertical

obstacles RectWall(4.5,1.0,4.8,4.9) і RectWall(7.5,2.4,7.8,4.9), as well as circular obstacles CircleObstacle(3.2,1.6,0.14), CircleObstacle(2.2,4.6,0.14), CircleObstacle(6.2,3.0,0.24), CircleObstacle(9.1,3.9,0.26) and a dynamic object of type "human" CircleObstacle(11.4,7.85,0.15) with a risk of 0.80, which has a small harmonic change in coordinates $x = 11.4 + 0.03\sin(0.55t)$, $y = 7.85 + 0.02\sin(0.80t + 0.5)$. LiDAR is modeled with 360 beams N_{rays} =360 with angles in the range $\Phi \in [-\pi, \pi]$, range $lidar_{\max\_range}$ =8.0 m and noise $lidar_{noise\_std}$ =0.01, the camera has a field of view $camera_{fov}$ =100° (≈1.745 rad) and range $camera_{range}$ =6.5m. VFH+ parameters are set to M =120 sectors, d_{max} =6.0 m, histogram w_d =1.0 and semantics w_s =1.00 weights, smoothing L =3, basic binarization threshold T_{base} =0.16 with adaptation to T =0.10…0.16 when "stuck", direction selection criterion weights μ_1 =3.2, μ_2 =1.0, μ_3 =0.9 and μ_{4_base} =0.90 with amplification up to $1.6 \cdot \mu_{4\_base}$ in stuck mode, and the minimum allowable valley distance changes to min_{valley_d} =0.26 or 0.22 in stuck mode. For control k_w =2.7, w_{max} =2.0rad/s, v_{max} =0.95 m/s, k_v =1.0 and v_{floor} =0.10m/s are used, and the global A* planner operates on a grid with a resolution of $grid_{res}$ =0.20m, inflations inflation_candidates=[d_{safe} +0.06, d_{safe} +0.03, d_{safe} +0.00, 0.18, 0.15, 0.12, 0.10] and wall extra inflation $wall_{extra}$ =0.18, with reproducibility ensured by a fixed random number generator seed=7.

The results of numerical modeling of the developed method of intelligent motion planning for a collaborative mobile robot in a dynamic environment based on VFH+ with semantic weighting of LiDAR and video data are presented in the form of graphs in Figures 1-3, and Figures 4-6 show the results of calculations.

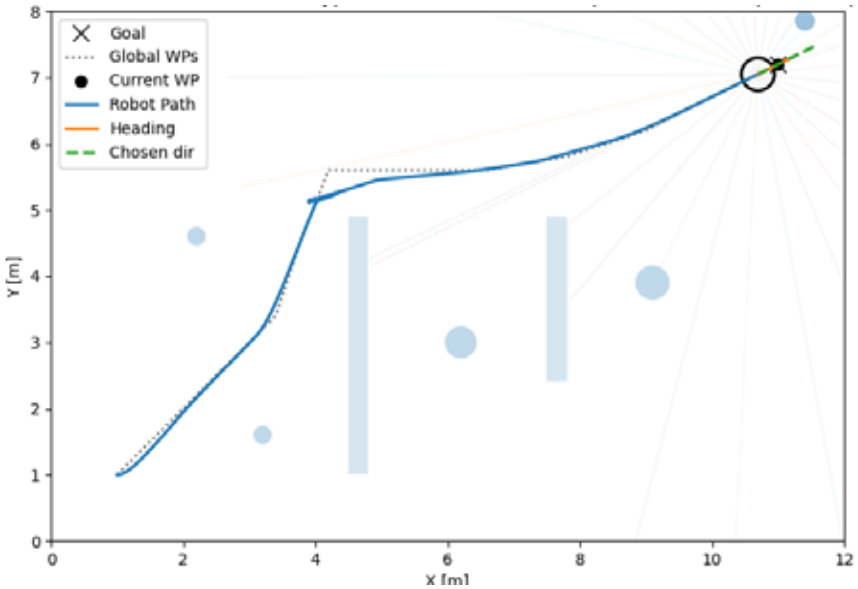

Fig. 1. Results of numerical modeling of route construction by a collaborative robot in a dynamic environment

As can be seen in Figure 1, the robot starts approximately from point $(x, y) \approx (1.0, 1.0)$ and successfully reaches the target $(11.0, 7.2)$, with the global distance "in a straight line" being about 11.8 m, and the actual length of the trajectory being greater (approximately 13–14 m) due to obstacle avoidance. The trajectory is consistent with the global waypoints: at $x \approx 4$ there is a visible active maneuver to bypass the first vertical wall (near 13–14м), after which the movement levels out and passes through the upper corridor with a smooth turn to the right side of the scene. In the area of the second vertical wall (near $x \approx 7.6$), the trajectory does not "stick" in the S-trap, but passes with a noticeable margin along $y \approx 5.5 - 6.0$, indicating sufficient passage width and correct operation of the "valleys/clearance" criteria. Near the target, the "chosen dir" vector practically coincides with the direction of movement, and local corrections do not lead to fluctuations, which qualitatively indicates the stabilization of VFH+ and adequate attenuation of speed/turn when approaching obstacles and the end point. Overall, the result demonstrates the balance between global A* (for strategic routing) and local VFH+ with semantics (for safe avoidance of dynamic or static objects) without critical stops or circular "spinning" in place.

From the Time-Series graph: $d_{min}(t), \sigma(d_{min}), v(t), w(t)$ (рис. 2) It is seen that at the initial stage of movement, the minimum distance to obstacles d_{min} exceeds 1.2–1.4 m, after which it decreases to approximately 0.35–0.45 m when entering the corridor, which corresponds to working in confined spaces, but without critically approaching the safety limit. The corresponding function $\sigma(d_{min})$ decreases to almost zero in narrow areas, which leads to an automatic reduction in linear speed $v(t)$ almost to 0–0.1 m/s and even short-term negative pulses corresponding to the escape mode or position correction. At moments of sharp decrease d_{min} peak angular velocity $w(t)$ values are observed up to ±2 rad/s, which shows active maneuvers to avoid obstacles and change orientation in difficult areas. After passing critical sections d_{min}

increases to 1.5–1.7 m, σ approaches 1, and the linear speed gradually returns to 0.8–1.0 m/s, indicating a transition to freer movement in open space. Fluctuations $w(t)$ in the final phase decrease in amplitude, which characterizes the stabilization of the trajectory as it approaches the target and the absence of self-oscillations or uncontrolled "twisting" in place. In general, time dependencies confirm the correct interaction of the gap assessment module, the deceleration function, and the orientation regulator within the adaptive VFH+ control.

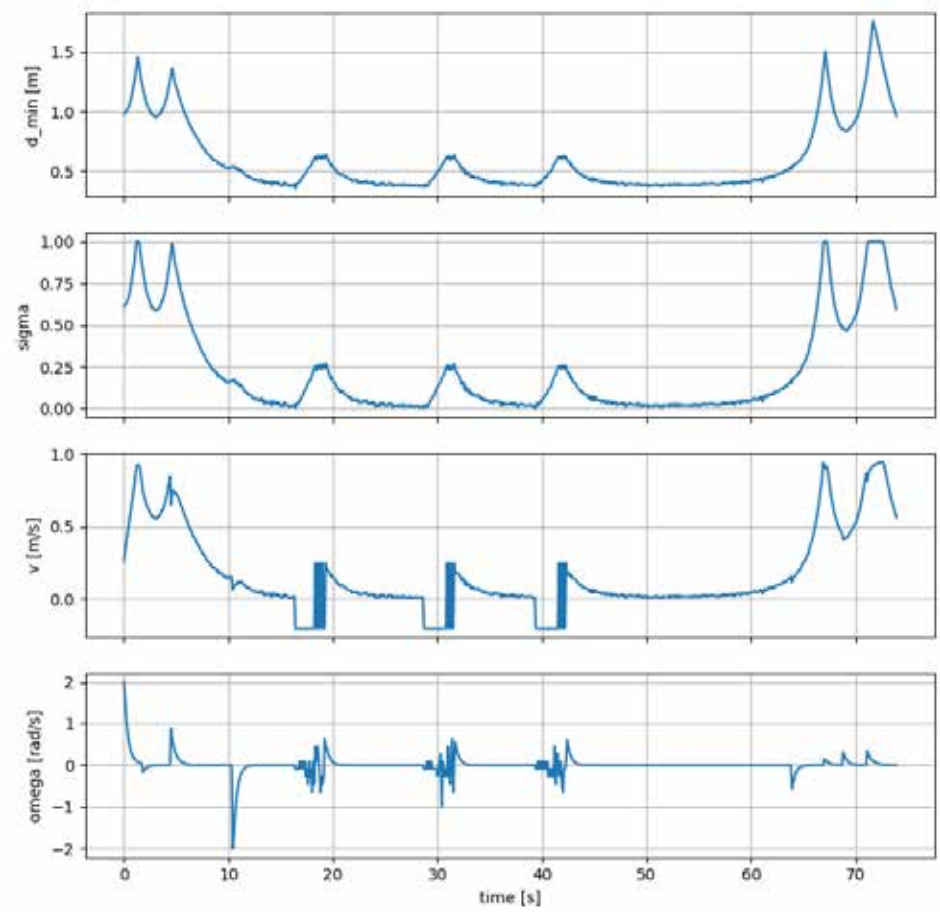

Fig. 2.Time-Series Graph: $d_{min}(t), \sigma(d_{min}), v(t), w(t)$

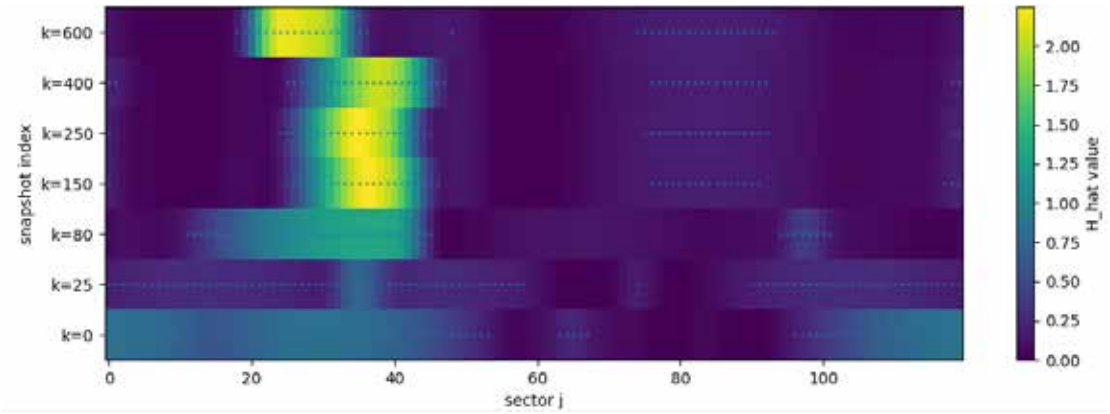

Fig. 3. Heatmap of $\tilde{H}_j$ over sectors (snapshots)

On the heat map (Fig. 3), histogram $\tilde{H}_j$ values ranging from approximately 0 to over 2.0 reflect the concentration of "risky" sectors at different points in time, with the most intense areas (yellow-green zones) observed in the sector interval close to $j \approx 30-45$ for the snapshots $k \approx 150-600$, corresponding to the passage of a narrow corridor between vertical

walls. At the initial moment $k = 0$, the distribution is more uniform and has moderate values, indicating a relatively free space in front of the robot. In the middle phase of movement, a compact "barrier" of sectors with increased $\tilde{H}_j$ is clearly formed, which shifts over time, reflecting the change in the relative position of obstacles in the field of view of the LiDAR and camera. After passing the critical zone, in the snapshots $k \geq 800$, the histogram values decrease and become localized in separate sectors, which corresponds to the exit into a more open space and an increase in d_{min}. The presence of sparse bright spots on the right side of the map is associated with the influence of a semantic obstacle of the "human" type, which forms narrow elevated risk sectors without completely blocking the passage. In general, the structure of the heat map confirms that the VFH+ algorithm forms a time-varying but stable profile of prohibited and safe directions, which adequately reflects the geometry and dynamics of the environment.

```
--- Global KEY waypoints (A*) ---
Inflation obs=0.430 m, wall=0.610 m, grid_res=0.20 m, waypoints=11
WP00: x=1.00, y=1.00
WP01: x=2.20, y=2.20
WP02: x=3.40, y=3.40
WP03: x=3.80, y=4.60
WP04: x=4.20, y=5.60
WP05: x=5.40, y=5.60
WP06: x=6.60, y=5.60
WP07: x=7.80, y=5.80
WP08: x=9.00, y=6.20
WP09: x=10.20, y=6.80
WP10: x=11.00, y=7.20
```

Fig. 4. Global KEY waypoints data (A*)

The resulting global route (Fig. 4) contains 11 key points from the start (1.0,1.0) to the destination (11.0,7. 2) with a grid resolution of 0.20 m and obstacle inflation of 0.43 m for circular objects and 0.61 m for walls, which provides an extended safety margin. The sequence of waypoints shows a smooth increase in coordinates along both the x and y axes, with the trajectory transitioning to an almost horizontal segment along $y \approx 5.6 - 5.8$ after point (4.2,5.6), corresponding to the passage through the upper corridor between the vertical walls. The distances between adjacent points are quasi-uniform and are approximately 1.2–1.4 m, which indicates correct discretization and further thinning of the global path. Qualitatively, the route does not contain any sharp changes in direction and provides a strategic bypass of internal obstacles with sufficient spatial reserve for local VFH+ correction.

```
--- Simulation start ---
Columns: step | x y th | v w | dist_wp dist_goal | dmin sigma | wp_i | stuck escape | T mu4 LOS
   0 | 1.026 1.000  0.200 |  0.26   2.00 |   1.70  11.77 | 0.98 0.61 |   1 |     0      0 | 0.16 0.90   1
   1 | 1.058 1.006  0.361 |  0.32   1.61 |   1.68  11.74 | 0.99 0.62 |   1 |     0      0 | 0.16 0.90   1
   2 | 1.094 1.020  0.482 |  0.38   1.21 |   1.65  11.71 | 0.99 0.62 |   1 |     0      0 | 0.16 0.90   1
   3 | 1.132 1.040  0.572 |  0.43   0.91 |   1.62  11.68 | 1.01 0.64 |   1 |     0      0 | 0.16 0.90   1
   4 | 1.173 1.066  0.641 |  0.49   0.69 |   1.58  11.63 | 1.03 0.66 |   1 |     0      0 | 0.16 0.90   1
   5 | 1.216 1.098  0.693 |  0.53   0.52 |   1.53  11.58 | 1.05 0.68 |   1 |     0      0 | 0.16 0.90   1
   6 | 1.260 1.135  0.733 |  0.58   0.40 |   1.48  11.53 | 1.08 0.71 |   1 |     0      0 | 0.16 0.90   1
   7 | 1.307 1.178  0.764 |  0.63   0.31 |   1.42  11.47 | 1.12 0.75 |   1 |     0      0 | 0.16 0.90   1
   8 | 1.357 1.225  0.788 |  0.69   0.24 |   1.36  11.41 | 1.16 0.79 |   1 |     0      0 | 0.16 0.90   1
   9 | 1.410 1.278  0.807 |  0.75   0.19 |   1.29  11.34 | 1.21 0.84 |   1 |     0      0 | 0.16 0.90   1
  10 | 1.464 1.335  0.822 |  0.79   0.15 |   1.21  11.27 | 1.24 0.87 |   1 |     0      0 | 0.16 0.90   1
  11 | 1.523 1.398  0.834 |  0.86   0.12 |   1.14  11.20 | 1.32 0.95 |   1 |     0      0 | 0.16 0.90   1
  15 | 1.766 1.673  0.864 |  0.91   0.06 |   0.77  10.85 | 1.35 0.98 |   1 |     0      0 | 0.16 0.90   1
  20 | 2.014 1.962  0.832 |  0.69  -0.10 |   2.07  10.47 | 1.12 0.75 |   2 |     0      0 | 0.16 0.90   1
  25 | 2.228 2.191  0.808 |  0.59  -0.03 |   1.74  10.16 | 1.00 0.63 |   2 |     0      0 | 0.16 0.90   1
```

Fig. 5. Modeling data at the initial stage

At the initial stage of modeling (Fig. 5), the robot moves from coordinates approximately (1.0, 1.0) with a gradual increase in the orientation angle to approximately 0.8–0.86 rad, which indicates an active turn in the direction of the first global waypoint. Minimum distance to obstacles d_{min} increases from 0.98 to over 1.3 m, and the coefficient increases to 0.95–0.98, allowing the linear velocity to increase to 0.8–0.9 m/s while simultaneously reducing the angular velocity. The stuck and escape indicators remain zero, and the T threshold and weight μ_4 are not adapted, which means there are no signs of jamming or critical narrowing of the passage. In general, the numerical values confirm the stable acceleration of the robot in conditions of sufficient space and the correct operation of the LOS check mechanism and local VFH+ control.

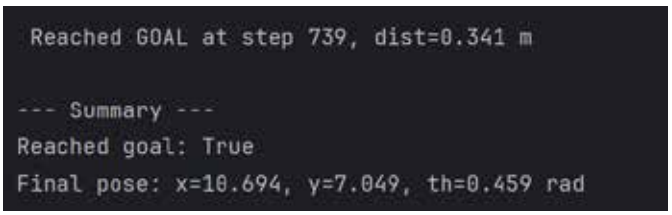

Fig. 6. Numerous modeling results

The modeling ended with the goal being achieved at step 739 with a residual distance of 0.341 m, which is less than the specified tolerance of 0.35 m and confirms the correct operation of the stop criterion. Final position of the robot $(x = 10.694, y = 7.049, \theta = 0.459 rad)$ is close to the specified point (11.0,7.2), and the orientation is consistent with the direction of the final approach. Taking into account the integration step of 0.1s, the total travel time is approximately 73.9s, which indicates a stable but safe pace of movement in a dynamic environment. The result demonstrates the absence of jamming, self-oscillation, or loss of global navigation strategy, and the integration of A* and adaptive VFH+ ensures guaranteed goal achievement while complying with safety restrictions.

Conclusions

In this work, a method for intelligent motion planning of a collaborative mobile robot in a dynamic environment based on the VFH+ algorithm with semantic weighting of LiDAR and video data was developed and investigated. Numerical modeling confirmed that the robot consistently reaches the target point (11.0; 7.2) when starting from coordinates (1.0; 1.0), and the actual length of the trajectory is about 13–14 m with a geometric distance in a straight line of about 11.8 m, which indicates correct obstacle avoidance and consistency of local VFH+ with global A* planning. The proposed integration of the polar histogram of obstacles with semantic weights made it possible to take into account not only the geometry of objects, but also their type and level of risk, which increased the adaptability and predictability of the robot's behavior in HRC scenarios. Control and planning parameters, in particular $k_w = 2.7$, $w_{max} = 2.0$ rad\s, $v_{max} = 0.95$ m\s, A grid resolution of 0.20 m and differentiated inflation of obstacles and walls ensured the reproducibility and stability of the algorithm under stochastic disturbances. The results confirm the effectiveness of combining global and local planning with semantic fusion of sensor data to improve the safety and reliability of mobile platforms in complex dynamic environments. The developed method is suitable for use in Industry 5.0 collaborative robotics systems, autonomous intra-shop logistics, service robots in public spaces, as well as in mobile robotic platforms for civil security and emergency rescue robots, where adaptability, predictability, and safe interaction with humans are critical.

Conflict of interest

The authors declare that they have no conflict of interest, in particular financial, personal, authorial or any other nature, which could affect the research, as well as the results published in this article.

Funding

Funding was provided within the framework of the implementation of the state theme "Hardware and software complex for detection and neutralization of explosive objects based on intelligent robotic platforms" at the Department of Computer Integrated Technologies, Automation, Robotics and Safety Engineering (CITARSE), Kharkiv National University of Radio Electronics.

Bibliography

1. Ma, D., Zhang, C., Xu, Q., & Zhou, G. Large and small-scale models' fusion-driven proactive robotic manipulation control for human-robot collaborative assembly in industry 5.0. *Robotics and Computer-Integrated Manufacturing.* 2026. 97, 103078. DOI: https://doi.org/10.1016/j.rcim.2025.103078.

2. Nevliudov, I., Omarov, M., Yevsieiev, V, Maksymova, S., & Jabrayilzade, E. MATHEMATICAL MODELING OF TRAJECTORIES CONSTRUCTION, MOVEMENT OF THE GRIPPING DEVICE OF A COLLABORATIVE ROBOT. *Advanced Information Systems.* 2026. 10(1), P. 11–20. DOI: https://doi.org/10.20998/2522-9052.2026.1.02.

3. Ghanghorkar, Y., Deshpande, A., & Misal, A. N. Human-robot interaction (HRI) and social robotics in industry 5.0: Drivers, barriers, and implications for sustainable development. *In Intelligent Systems for Neurocognition and*

Human-Robot-Computer Interaction. Academic Press. 2026. P. 127-152. DOI: https://doi.org/10.1016/B978-0-443-41660-6.00013-2.

4. Nevliudov, I., Yevsieiev, V., Maksymova, S., Gopejenko, V., & Kosenko, V. DEVELOPMENT OF MATHEMATICAL SUPPORT FOR ADAPTIVE CONTROL FOR THE INTELLIGENT GRIPPER OF THE COLLABORATIVE ROBOT MANIPULATOR. *Advanced Information Systems*. 2025 9(3), P. 57–65. DOI: https://doi.org/10.20998/2522-9052.2025.3.07.

5. Liu, S., Xie, J., Wang, X., & Qiao, X. You are my eyes: Integrating human intelligence and LLMs in AR-assisted motion planning for industrial mobile robots. *Robotics and Computer-Integrated Manufacturing*. 2026. 98, 103174. DOI: https://doi.org/10.1016/j.rcim.2025.103174.

6. Yang, H., Xu, W., Pham, D. T., Qi, L., & Ba, M. Decentralised task planning and motion coordination for scalable multi-robot collaborative manufacturing. *Robotics and Computer-Integrated Manufacturing.* 2026. 100, 103255. DOI: https://doi.org/10.1016/j.rcim.2026.103255.

7. Amer Abu-Jassar, Hassan Al-Sukhni, Yasser Al-Sharo, Svitlana Maksymova, Vladyslav Yevsieiev, Vyacheslav Lyashenko, Building a Route for a Mobile Robot Based on the BRRT and A*(H-BRRT) Algorithms for the Effective Development of Technological Innovations. *International Journal of Engineering Trends and Technology*. 2024. Vol. 72, no. 11, P. 294-306, DOI: https://doi.org/10.14445/22315381/IJETT-V72I11P129.

8. Huang, S. Human-Robot Collaborative Path Planning with Predictive Obstacle Avoidance. *Intelligent & Human Futures.* 2026. 2(1), P. 1-12. DOI: https://doi.org/10.63808/ihf.v2i1.268.

9. Zhang, J., Su, L., Bai, Z., Yang, S. X., Li, P., Hong, S., … & Song, L. Research on Path Planning and Trajectory Tracking for Inspection Robots in Orchard Environments. *Agriculture.* 2026. 16(4), 415. DOI: https://doi.org/10.3390/agriculture16040415.

10. Jiang, W., Liu, J., Wang, W., & Wang, Y. Global Path Planning for Land–Air Amphibious Biomimetic Robot Based on Improved PPO. *Biomimetics.* 2026 11(1), 25. DOI: https://doi.org/10.3390/biomimetics11010025.

11. Li, Z., Kou, D., Wang, Y., Li, W., Dong, Z., & Zhang, L. Auto-Follower: A Person-Following System for Urban Ackermann Human–Machine Collaborative Robotics. *ACM Transactions on Autonomous and Adaptive Systems*. 2025. DOI: https://doi.org/10.1145/3787977.

12. Katikaridis, D., Benos, L., Kateris, D., Papageorgiou, E., Karras, G., Menexes, I., … & Bochtis, D. Proactive Path Planning Using Centralized UAV-UGV Coordination in Semi-Structured Agricultural Environments. *Applied Sciences*. 2026. 16(2), 1143. https://doi.org/10.3390/app16021143.

13. Basnet, S., Andersen, J. C., & Boukas, E. Design and Implementation of a Low-Cost Perception System for Aerial Robots in Confined Spaces. *Sensors*. 2026. 26(4), 1140. DOI: https://doi.org/10.3390/s26041140.

14. Sellers, T., Lei, T., Wang, J., Iqbal, U., Liu, L., & Luo, C. Advancing Robot Local Navigation Through Vector Field Histograms Using a Hybrid Learning Approach. *In 2025 IEEE Frontiers in Education Conference (FIE).* 2025. IEEE. P. 1-9. DOI: https://doi.org/10.1109/FIE63693.2025.11328231.

15. Shili, M., Chaoui, H., & Nouri, K. Energy-aware sensor fusion architecture for autonomous channel robot navigation in constrained environments. *Sensors*. 2025. 25(21), 6524. DOI: https://doi.org/10.3390/s25216524.

16. Liang, W., Ji, Y., Sun, X., Liu, X., & Wu, J. Multi-agent VFH+ flocking control with escaping dynamic equilibrium under complex obstacles. *Complex & Intelligent Systems.* 2025. 11(11), 467. DOI: https://doi.org/10.1007/s40747-025-02100-7.

17. Rose, C., McMurray, R., & Hadi, M. U. Field-based Autonomous LiDAR Control for Obstacle Navigation (FALCON). *In 2025 35th Irish Signals and Systems Conference (ISSC)*. 2025. IEEE. P. 1-6. DOI: https://doi.org/10.1109/ISSC67739.2025.11291231.

18. Hu, D., & Gan, V. J. Semantic navigation for automated robotic inspection and indoor environment quality monitoring. *Automation in Construction.* 2025. 170, 105949. DOI: https://doi.org/10.1016/j.autcon.2024.105949.

19. Gutiérrez-Álvarez, C., Rios-Navarro, P., Flor-Rodriguez-Rabadan, R., Acevedo-Rodriguez, F. J., & Lopez-Sastre, R. J. Visual semantic navigation with real robots. *Applied Intelligence.* 2025. 55(3), 206. DOI: https://doi.org/10.1007/s10489-024-06115-4.

20. Shen, Z., Luo, H., Chen, K., Lv, F., & Li, T. Enhancing multi-robot semantic navigation through multimodal chain-of-thought score collaboration. *In Proceedings of the AAAI Conference on Artificial Intelligence.* 2025. Vol. 39, No. 14, P. 14664-14672. DOI: https://doi.org/10.1609/aaai.v39i14.33607.

21. Yang, G., An, L., & Zhao, C. Collision/obstacle avoidance coordination of multi-robot systems: A survey. *In Actuators.* 2025. Vol. 14, No. 2, P. 85. MDPI. DOI: https://doi.org/10.3390/act14020085.

22. Wei, Z., Wang, S., Chen, K., & Wang, F. Ros-based navigation and obstacle avoidance: A study of architectures, methods, and trends. *Sensors.* 2025. 25(14), 4306. DOI: https://doi.org/10.3390/s25144306.

23. Misir, O., & Celik, M. Visual-based obstacle avoidance method using advanced CNN for mobile robots. *Internet of Things*. 2025 31, 101538. DOI: https://doi.org/10.1016/j.iot.2025.101538.

24. Sousa, L. C., Silva, Y. M., Schettino, V. B., Santos, T. M., Zachi, A. R., Gouvêa, J. A., & Pinto, M. F. Obstacle avoidance technique for mobile robots at autonomous human-robot collaborative warehouse environments. *Sensors*. 2025. 25(8), 2387. DOI: https://doi.org/10.3390/s25082387.

25. NT, S. K., & Rajalakshami, P. Optimized Real-Time Path Planning and Obstacle Avoidance for Dynamic Objects Using a Velocity-Based Approach. *In 2025 9th International Conference on Robotics and Automation Sciences (ICRAS)*. 2025. IEEE. P. 178-183. DOI: https://doi.org/10.1109/ICRAS65818.2025.11108762.

26. Wang, H., Li, Y., Yan, J., Xiao, W., Han, S., & Liu, Y. A novel minute-scale prediction method of incoming wind conditions with limited LiDAR data. *Renewable Energy*. 2025. 240, 122235. DOI: https://doi.org/10.1016/j.renene.2024.122235.

27. Al-Sharo, Y., Abu-Jassar, A., Lyashenko, V., Yevsieiev, V., & Maksymova, S. A Robo-hand prototype design gripping device within the framework of sustainable development. *Indian Journal of Engineering*. 2023. 20, e37ije1673. DOI: https://doi.org/10.54905/disssi.v20i54.e37ije1673.

28. Yevsieiev, V., Gurin, D., Kulish, S., & Voloshyn, Y. Development of a partially supervised Markov decision-making model for a 3-link collaborative robot-manipulator. *Radioelectronic and Computer Systems.* 2025. 2025(4), 83-94. DOI: https://doi.org/10.32620/reks.2025.4.06.

29. Corrêa, A. B., Pereira, A. G., & Seipp, J. Classical planning with llm-generated heuristics: Challenging the state of the art with python code. *arXiv preprint arXiv:2503*. 2025. 18809. https://doi.org/10.48550/arXiv.2503.18809.

References

1. Ma, D., Zhang, C., Xu, Q., & Zhou, G. (2026). Large and small-scale models' fusion-driven proactive robotic manipulation control for human-robot collaborative assembly in industry 5.0. Robotics and Computer-Integrated Manufacturing, 97, 103078. https://doi.org/10.1016/j.rcim.2025.103078

2. Nevliudov, I., Omarov, M., Yevsieiev, V, Maksymova, S., & Jabrayilzade, E. (2026). MATHEMATICAL MODELING OF TRAJECTORIES CONSTRUCTION, MOVEMENT OF THE GRIPPING DEVICE OF A COLLABORATIVE ROBOT. Advanced Information Systems, 10(1), 11–20. https://doi.org/10.20998/2522-9052.2026.1.02

3. Ghanghorkar, Y., Deshpande, A., & Misal, A. N. (2026). Human-robot interaction (HRI) and social robotics in industry 5.0: Drivers, barriers, and implications for sustainable development. In Intelligent Systems for Neurocognition and Human-Robot-Computer Interaction (pp. 127-152). Academic Press. https://doi.org/10.1016/B978-0-443-41660-6.00013-2

4. Nevliudov, I., Yevsieiev, V., Maksymova, S., Gopejenko, V., & Kosenko, V. (2025). DEVELOPMENT OF MATHEMATICAL SUPPORT FOR ADAPTIVE CONTROL FOR THE INTELLIGENT GRIPPER OF THE COLLABORATIVE ROBOT MANIPULATOR. Advanced Information Systems, 9(3), 57–65. https://doi.org/10.20998/2522-9052.2025.3.07

5. Liu, S., Xie, J., Wang, X., & Qiao, X. (2026). You are my eyes: Integrating human intelligence and LLMs in AR-assisted motion planning for industrial mobile robots. Robotics and Computer-Integrated Manufacturing, 98, 103174. https://doi.org/10.1016/j.rcim.2025.103174

6. Yang, H., Xu, W., Pham, D. T., Qi, L., & Ba, M. (2026). Decentralised task planning and motion coordination for scalable multi-robot collaborative manufacturing. Robotics and Computer-Integrated Manufacturing, 100, 103255. https://doi.org/10.1016/j.rcim.2026.103255

7. Amer Abu-Jassar, Hassan Al-Sukhni, Yasser Al-Sharo, Svitlana Maksymova, Vladyslav Yevsieiev, Vyacheslav Lyashenko, "Building a Route for a Mobile Robot Based on the BRRT and A*(H-BRRT) Algorithms for the Effective Development of Technological Innovations," International Journal of Engineering Trends and Technology, vol. 72, no. 11, pp. 294-306, 2024. Crossref, https://doi.org/10.14445/22315381/IJETT-V72I11P129

8. Huang, S. (2026). Human-Robot Collaborative Path Planning with Predictive Obstacle Avoidance. Intelligent & Human Futures, 2(1), 1-12. https://doi.org/10.63808/ihf.v2i1.268

9. Zhang, J., Su, L., Bai, Z., Yang, S. X., Li, P., Hong, S., … & Song, L. (2026). Research on Path Planning and Trajectory Tracking for Inspection Robots in Orchard Environments. Agriculture, 16(4), 415. https://doi.org/10.3390/agriculture16040415

10. Jiang, W., Liu, J., Wang, W., & Wang, Y. (2026). Global Path Planning for Land–Air Amphibious Biomimetic Robot Based on Improved PPO. Biomimetics, 11(1), 25. https://doi.org/10.3390/biomimetics11010025

11. Li, Z., Kou, D., Wang, Y., Li, W., Dong, Z., & Zhang, L. Auto-Follower: A Person-Following System for Urban Ackermann Human–Machine Collaborative Robotics. ACM Transactions on Autonomous and Adaptive Systems. https://doi.org/10.1145/3787977

12. Katikaridis, D., Benos, L., Kateris, D., Papageorgiou, E., Karras, G., Menexes, I., … & Bochtis, D. (2026). Proactive Path Planning Using Centralized UAV-UGV Coordination in Semi-Structured Agricultural Environments. Applied Sciences, 16(2), 1143. https://doi.org/10.3390/app16021143

13. Basnet, S., Andersen, J. C., & Boukas, E. (2026). Design and Implementation of a Low-Cost Perception System for Aerial Robots in Confined Spaces. Sensors, 26(4), 1140. https://doi.org/10.3390/s26041140

14. Sellers, T., Lei, T., Wang, J., Iqbal, U., Liu, L., & Luo, C. (2025, November). Advancing Robot Local Navigation Through Vector Field Histograms Using a Hybrid Learning Approach. In 2025 IEEE Frontiers in Education Conference (FIE) (pp. 1-9). IEEE. https://doi.org/10.1109/FIE63693.2025.11328231

15. Shili, M., Chaoui, H., & Nouri, K. (2025). Energy-aware sensor fusion architecture for autonomous channel robot navigation in constrained environments. Sensors, 25(21), 6524. https://doi.org/10.3390/s25216524

16. Liang, W., Ji, Y., Sun, X., Liu, X., & Wu, J. (2025). Multi-agent VFH+ flocking control with escaping dynamic equilibrium under complex obstacles. Complex & Intelligent Systems, 11(11), 467. https://doi.org/10.1007/s40747-025-02100-7

17. Rose, C., McMurray, R., & Hadi, M. U. (2025, June). Field-based Autonomous LiDAR Control for Obstacle Navigation (FALCON). In 2025 35th Irish Signals and Systems Conference (ISSC) (pp. 1-6). IEEE. https://doi.org/10.1109/ISSC67739.2025.11291231

18. Hu, D., & Gan, V. J. (2025). Semantic navigation for automated robotic inspection and indoor environment quality monitoring. Automation in Construction, 170, 105949. https://doi.org/10.1016/j.autcon.2024.105949

19. Gutiérrez-Álvarez, C., Rios-Navarro, P., Flor-Rodriguez-Rabadan, R., Acevedo-Rodriguez, F. J., & Lopez-Sastre, R. J. (2025). Visual semantic navigation with real robots: C. Gutiérrez-Álvarez et al. Applied Intelligence, 55(3), 206. https://doi.org/10.1007/s10489-024-06115-4

20. Shen, Z., Luo, H., Chen, K., Lv, F., & Li, T. (2025, April). Enhancing multi-robot semantic navigation through multimodal chain-of-thought score collaboration. In Proceedings of the AAAI Conference on Artificial Intelligence (Vol. 39, No. 14, pp. 14664-14672). https://doi.org/10.1609/aaai.v39i14.33607

21. Yang, G., An, L., & Zhao, C. (2025, February). Collision/obstacle avoidance coordination of multi-robot systems: A survey. In Actuators (Vol. 14, No. 2, p. 85). MDPI. https://doi.org/10.3390/act14020085

22. Wei, Z., Wang, S., Chen, K., & Wang, F. (2025). Ros-based navigation and obstacle avoidance: A study of architectures, methods, and trends. Sensors, 25(14), 4306. https://doi.org/10.3390/s25144306

23. Misir, O., & Celik, M. (2025). Visual-based obstacle avoidance method using advanced CNN for mobile robots. Internet of Things, 31, 101538. https://doi.org/10.1016/j.iot.2025.101538

24. Sousa, L. C., Silva, Y. M., Schettino, V. B., Santos, T. M., Zachi, A. R., Gouvêa, J. A., & Pinto, M. F. (2025). Obstacle avoidance technique for mobile robots at autonomous human-robot collaborative warehouse environments. Sensors, 25(8), 2387. https://doi.org/10.3390/s25082387

25. NT, S. K., & Rajalakshami, P. (2025, June). Optimized Real-Time Path Planning and Obstacle Avoidance for Dynamic Objects Using a Velocity-Based Approach. In 2025 9th International Conference on Robotics and Automation Sciences (ICRAS) (pp. 178-183). IEEE. https://doi.org/10.1109/ICRAS65818.2025.11108762

26. Wang, H., Li, Y., Yan, J., Xiao, W., Han, S., & Liu, Y. (2025). A novel minute-scale prediction method of incoming wind conditions with limited LiDAR data. Renewable Energy, 240, 122235. https://doi.org/10.1016/j.renene.2024.122235

27. Al-Sharo, Y., Abu-Jassar, A., Lyashenko, V., Yevsieiev, V., & Maksymova, S. (2023). A Robo-hand prototype design gripping device within the framework of sustainable development. Indian Journal of Engineering, 20, e37ije1673. https://doi.org/10.54905/disssi.v20i54.e37ije1673

28. Yevsieiev, V., Gurin, D., Kulish, S., & Voloshyn, Y. (2025). Development of a partially supervised Markov decision-making model for a 3-link collaborative robot-manipulator. Radioelectronic and Computer Systems, 2025(4), 83-94. https://doi.org/10.32620/reks.2025.4.06

29. Corrêa, A. B., Pereira, A. G., & Seipp, J. (2025). Classical planning with llm-generated heuristics: Challenging the state of the art with python code. arXiv preprint arXiv:2503.18809. https://doi.org/10.48550/arXiv.2503.18809

Дата першого надходження статті до видання: 10.02.2026
Дата прийняття статті до друку після рецензування: 13.03.2026
Дата публікації (оприлюднення) статті: 07.05.2026